



Evidence of a SARS-CoV-2 double Spike mutation D614G/S939F potentially affecting immune response of infected subjects



Sara Donzelli^a, Francesca Spinella^b, Enea Gino di Domenico^c, Martina Pontone^c, Ilaria Cavallo^c, Giulia Orlandiⁿ, Stefania Iannazzo^d, Giulio Maria Ricciuto^e, ISG Virology Covid Team^{c,1}, Raul Pellini^f, Paola Muti^g, Sabrina Strano^h, Gennaro Cilibertoⁱ, Fabrizio Ensoli^c, Stefano Zapperi^{j,k}, Caterina A.M. La Porta^{l,m}, Giovanni Blandino^{a,*}, Aldo Morroneⁿ, Fulvia Pimpinelli^{c,*}

^a Oncogenomic and Epigenetic Unit, IRCCS Regina Elena National Cancer Institute, Rome, Italy

^b Eurofins Genoma Group Srl, Via di Castel Giubileo, 11, 00138 Rome, Italy

^c Department of Microbiology and Virology, IRCCS San Gallicano Dermatological Institute, Rome, Italy

^d Department of Prevention, Hygiene and Public Health ASL RM 3, Rome, Italy

^e Emergency Department ASL Rome 3, GB Grassi Hospital, Ostia Lido, Rome, Italy

^f Department Otolaryngology Head and Neck Surgery, IRCCS Regina Elena National Cancer Institute, Rome, Italy

^g Department of Biomedical, Surgical and Dental Sciences, "Università degli Studi di Milano", Milan, Italy

^h SAFU Unit, IRCCS Regina Elena National Cancer Institute, Rome, Italy

ⁱ Scientific Direction, IRCCS Regina Elena National Cancer Institute, Rome, Italy

^j Center for Complexity and Biosystems, Department of Physics, University of Milan, Via Celoria 16, 20133 Milano, Italy

^k CNR – Consiglio Nazionale delle Ricerche, Istituto di Chimica della Materia Condensata e di Tecnologie per l'Energia, via R. Cozzi 53, 20125 Milano, Italy

^l Center for Complexity and Biosystems, Department of Environmental Science and Policy, University of Milan, via Celoria 26, 20133 Milano, Italy

^m CNR – Consiglio Nazionale delle Ricerche, Istituto di Biofisica, via Celoria 26, 20133 Milano, Italy

ⁿ Scientific Direction, IRCCS San Gallicano Dermatological Institute, Rome, Italy

ARTICLE INFO

Article history:

Received 7 July 2021

Received in revised form 18 January 2022

Accepted 18 January 2022

Available online 21 January 2022

Keywords:

SARS-CoV-2

Spike mutations

D614G

S939F

Immune response

ABSTRACT

Objectives: Despite extensive efforts to monitor the diffusion of COVID-19, the actual wave of infection is worldwide characterized by the presence of emerging SARS-CoV-2 variants. The present study aims to describe the presence of yet undiscovered SARS-CoV-2 variants in Italy.

Methods: Next Generation Sequencing was performed on 16 respiratory samples from occasionally employed within the Bangladeshi community present in Ostia and Fiumicino towns. Computational strategy was used to identify all potential epitopes for reference and mutated Spike proteins. A simulation of proteasome activity and the identification of possible cleavage sites along the protein guided to a combined score involving binding affinity, peptide stability and T-cell propensity.

Results: Retrospective sequencing analysis revealed a double Spike D614G/S939F mutation in COVID-19 positive subjects present in Ostia while D614G mutation was evidenced in those based in Fiumicino. Unlike D614G, S939F mutation affects immune response by the slight but significant modulation of T-cell propensity and the selective enrichment of potential binding epitopes for some HLA alleles.

Conclusion: Collectively, our findings mirror further the importance of deep sequencing of SARS-CoV-2 genome as a unique approach to monitor the appearance of specific mutations as for those herein reported for Spike protein. This might have implications on both the type of immune response triggered by the viral infection and the severity of the related illness.

© 2022 The Author(s). Published by Elsevier B.V. on behalf of Research Network of Computational and Structural Biotechnology. This is an open access article under the CC BY license (<http://creativecommons.org/licenses/by/4.0/>).

* Corresponding authors.

E-mail addresses: giovanni.blandino@ifo.gov.it (G. Blandino), fulvia.pimpinelli@ifo.gov.it (F. Pimpinelli).

¹ ISG Virology Covid Team: Cavallo Ilaria, Cazzani Andrea, Celesti Ilaria, D'Agosto Giovanna, Diano Martina, Federico Antonio, Fraticelli Fulvia, Furzi Lorenzo, Giuliani Eugenia, Lauretti Alessia, Maione Francesca, Mastrofrancesco Arianna, Obregon Francisco, Paluzzi Silvia, Petrolo Sara, Prignano Grazia, Ricca Valentina, Salvo Serena, Tatangelo Miriam, Trento Elisabetta, Zucchiatti Marco.

<https://doi.org/10.1016/j.csbj.2022.01.021>

2001-0370/© 2022 The Author(s). Published by Elsevier B.V. on behalf of Research Network of Computational and Structural Biotechnology.

This is an open access article under the CC BY license (<http://creativecommons.org/licenses/by/4.0/>).

1. Introduction

Betacoronaviruses are responsible of the last three major pathogenic zoonotic diseases occurred in the past two decades [1]. Indeed, severe acute respiratory syndrome (SARS-CoV) emerged in 2002 and exhibited 10% mortality of infected people [2]. Middle East respiratory syndrome coronavirus (MERS-CoV) appeared in 2012 with 35% mortality [3]. To date, SARS-CoV-2 records world-

A

Table 1. Consensus sequences of study samples: differences vs. Wuhan-Hu-1sequence															
PT															
Region	nt	rf	BAN				BAN				FIU				M-AA changes
			BANG-1B_	G-2B_	BANG-3B_	BANG-4B_	G-5B_	BANG-6B_	BANG-7B_	BANG-8B_	FIUM-3A_	FIUM-5A_	FIUM-7A_	FIUM-8A_	
	25	T													
UTR	105	G	T		T	T	T	T	T	T					
	241	C	T	T	T	T	T	T	T	T	T	T	T	T	
	1163	A	T	T	T	T	T	T	T	T	T	T	T	T	I300F
	3037	C	T	T	T	T	T	T	T	T	T	T	T	T	Syn
	7798A	G													Syn
	11083	G	T												L3606F
	11719	G			T	T			T						Q3818H
	14408	C	T		T	T	T	T	T	T	T	T	T	T	P314L
	15738	C		T						T	T	T	T	T	Syn
	16718	G		A						A	A	A	A	A	R1084K
Orf1ab	17999	C		T						T	T	T	T	T	T1511I
	23403	A	G	G	G	G	G	G	G	G	G	G	G	G	D614G
S	24378	C	T		T	T	T	T	T						S939F
	28881	G	A	A	A	A	A	A	A	A	A	A	A	A	R203K
	28882	G	A	A	A	A	A	A	A	A	A	A	A	A	Syn
N	28883	G	C	C	C	C	C	C	C	C	C	C	C	C	G204R
	ORF14	29840	T												G50R
	29848	T												A	Syn
	29841	G		T											G50E
	29830	G			T										Syn

nt, nucleotide; AA, amino acid; Syn, synonymous substitution; UTR, untranslated region; Orf, open reading fra; S, Spike protein

B

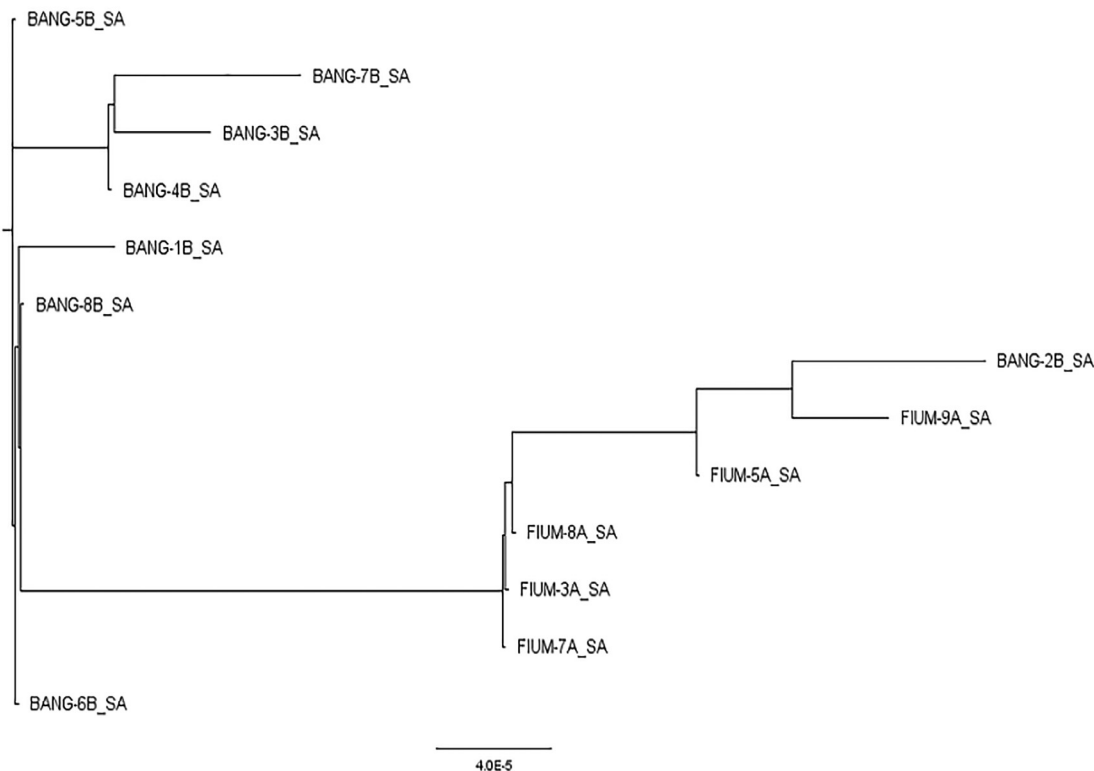
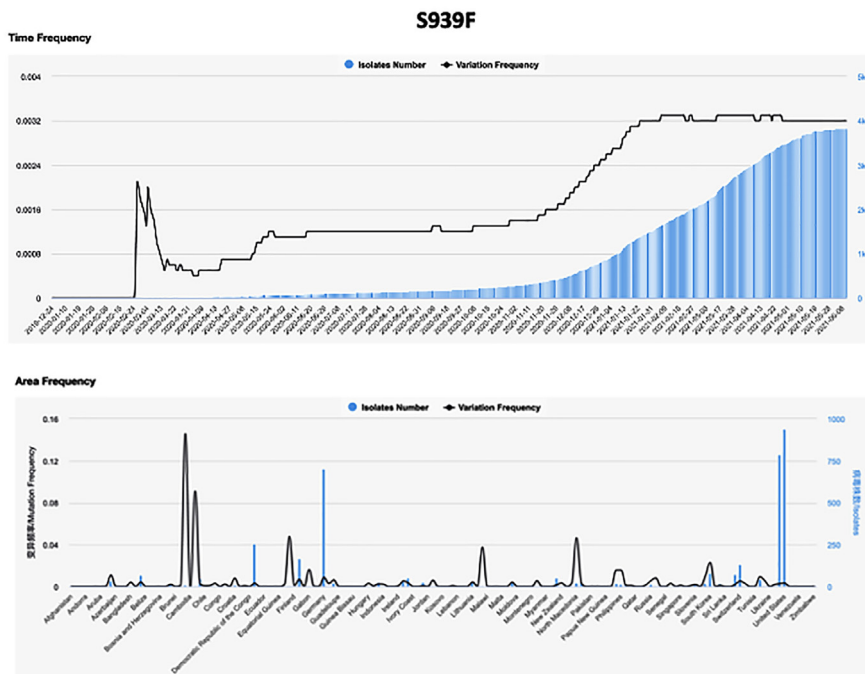


Fig. 1. Genetic Variability and phylogenetic analysis of Whole-Genome Consensus Sequences. A. For the mutations analysis, sequences of viral genomes and the reference sequence (GenBank ID NC_045512.2) were aligned with Clustal Omega [31,32] and analyzed with MEGA X [33]. Nucleotide positions are referred to Wuhan-Hu-1(reference genome MN908947). B. For phylogenetic analysis, we inferred the maximum-likelihood tree using the edge-linked partition model in IQ-TREE (<http://www.iqtree.org/>) [34,35].

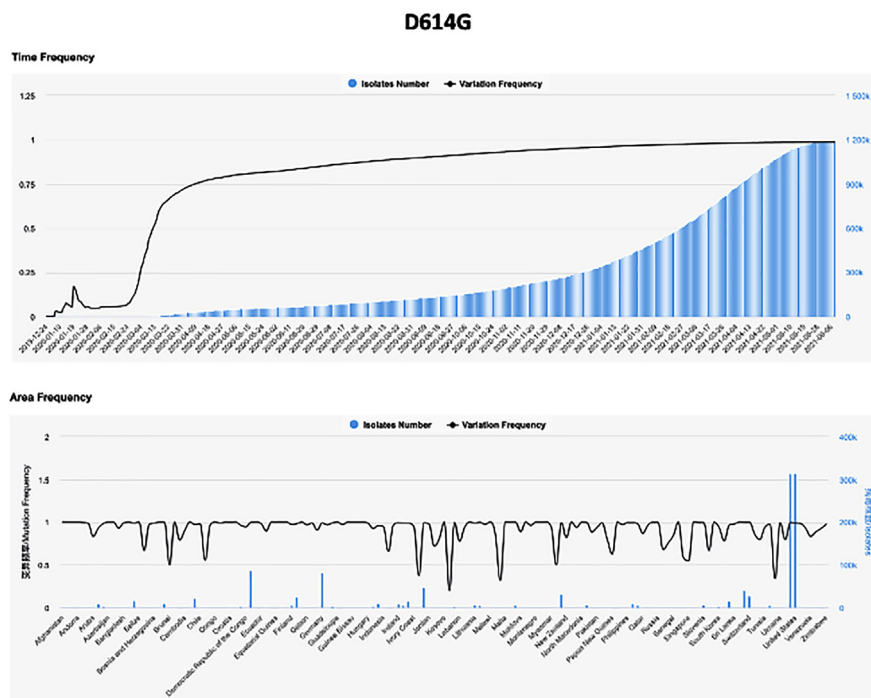
A

Amino acid mutated	Genome position	Gene name	Virus number with variation	Annotation Type	Mutation Type	Base change:Virus number	Evidence Level	Variance Time	Variance Area	Impact Ensembl Variation - Calculated variant consequences
S939	24378	S	1316	missense_variant; coding_sequence_variant	SNP	C>M:2; C>G:1; C>T:3853; C>A:18; C>Y:30	IV	1.23E-06	2.34E-04	MODERATE; MODIFIER
D614	23403	S	454687	missense_variant; coding_sequence_variant	SNP	A>M:1; A>G:1218522; A>R:93; A>C:14	I	8.34E-02	2.23E-02	MODERATE; MODIFIER

B



C



wide over than 80 millions of infected people with around 2 millions deaths. Since SARS-CoV-2 pandemic is still active, the related numbers grow daily. Coronavirus entry into host cells is pivotal for viral infectivity and pathogenesis. It also represents of major determinant for immune surveillance and a key target for therapeutic intervention. SARS-CoV-2 enters host cells of high and low respiratory tracts binding ACE2, a cell surface receptor for viral attachment [4]. Subsequently TMPRSS2 internalization protease primes S protein [4]. SARS-CoV S1 contains a Receptor-binding domain (RBD) that specifically binds to hACE2 receptor. RBD status constantly oscillates between standing-up conformation for receptor binding to lying-down position for immune evasion [5]. The crystal structure of the complex between SARS-CoV-2 RBD and h-ACE2 receptor has been recently solved [6]. It revealed subtle differences between previously identified SARS-Co-V RBD and SARS-CoV-2 RBD to recognize hACE2. This leads to the increased binding affinity of SARS-CoV-2 to the receptor and determines its severe effects of the infected cell types. Moreover, compared with other SARS-related coronaviruses (SARSr-CoVs), SARS-CoV-2 possesses a unique furin cleavage site (FCS) in its spike protein that is highly functional and that increases the efficiency of virus infection into cells [7].

Herein we identified by retrospective next-generation sequencing analysis a SARS-CoV-2 double Spike mutation D614G/S939F in 16 respiratory samples from occasionally employers within the Bangladeshi community present in Ostia. SARS-CoV-2 Spike D614G mutation was evidenced in the members of the Bangladeshi community living in the close town Fiumicino who were frequently in contact with those members found positive for Spike D614G/S939F double mutation in Ostia. We also found that unlike D614G, S939F mutation affects immune response through the slight but significant modulation of T-cell propensity and the selective enrichment of potential binding epitopes for some HLA alleles.

2. Results

2.1. Identification of a SARS-CoV-2 double Spike mutation D614G/S939F

RA, a 44-year old male from Bangladesh was admitted at the Emergency Unit of Grassi Hospital in Ostia-ASL Rome 3 on 7.16.2020 with the following clinical parameters and symptoms: normal ECG, oxygen saturation values of 97%, fever and left flank pain. The patient referred, exhibited evident signs of pneumonia and tested positive for SARS-CoV-2 infection. Since RA lived in Ostia in the same house with 8 members of the Bangladeshi community, the COVID-19 team of ASL-Rome 3 tracked and tested all members of SARS-CoV-2 infection. All roommates tested positive for SARS-CoV-2 infection but unlike RA did not show any evident sign of pneumonia. The molecular detection of SARS-CoV-2 was performed at the Virology and Microbiology Unit of San Gallicano Institute in Rome. For working reasons some of the members of the Bangladeshi group in Ostia interacted frequently with a group of Bangladeshi workers located in Fiumicino, a city of 80,000 habi-

tants located at 25 miles from Rome. All these identified co-workers were assessed for SARS-CoV-2 infection on July 2020 and tested positive. All SARS-CoV-2 positive subjects left Italy during the lockdown period (March to May 2020) and returned in Bangladesh. They came back to Italy at the beginning of June 2020 and were occasionally employed in Ostia and Fiumicino. We do not have any records regarding previously swabs performed in Bangladesh. Both, their return to Italy from Bangladesh soon after the Italian lockdown and their occasional employment at different site in Italy prompted us to sequence their SARS-CoV-2 genome and consequently to monitor the potential presence of previously unidentified viral variants. To this end Next Generation Sequencing analysis was performed on 16 respiratory samples (six NPS and seven BAL) from 16 patients obtaining on average 2.0×10^6 reads per sample (range $0.8\text{--}4.2 \times 10^6$). Mean value and range of coverage for SARS-CoV-2 genome of reads obtained by NGS for each analyzed sample are represented in Supplementary Table 1.

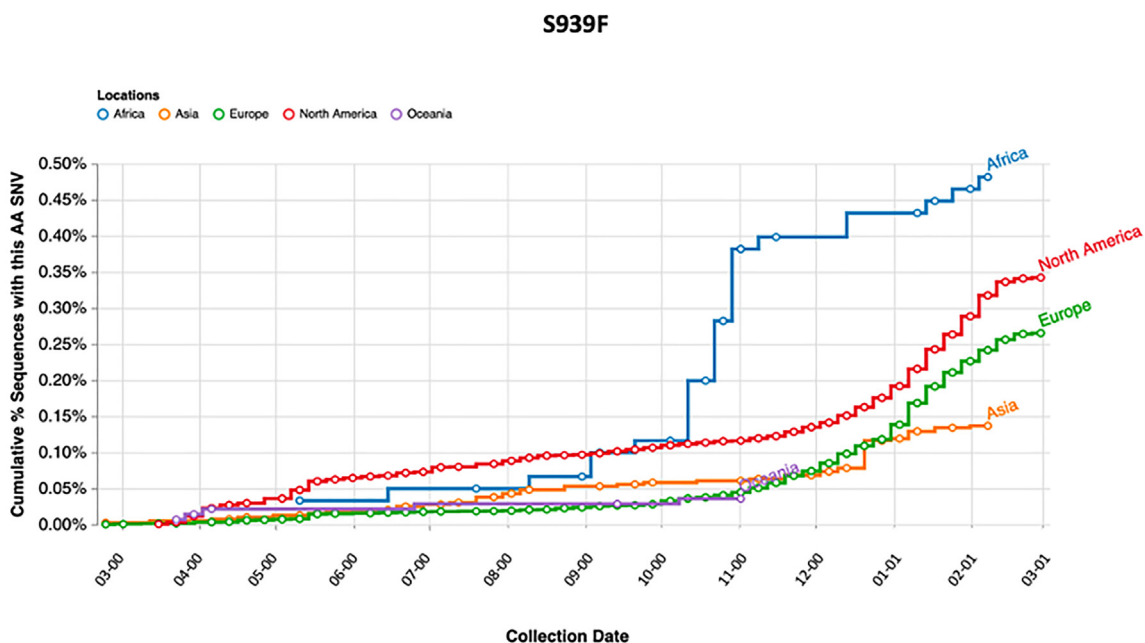
Consensus sequences are described in the table in Fig. 1A, and differences with the Wuhan-Hu reference genome (GenBank: MN908947) are highlighted. We obtained 13 complete genomes (Fig. 1A). Consensus genomes had a median of 8 substitutions relative to the Wuhan-Hu-1/2019 reference sequence (range 7–10). For phylogenetic analysis, we inferred the maximum-likelihood tree using the edge-linked partition model in IQ-TREE and we identified 2 unique evolutionary lineages in our cohort (lineages was built on the basis of the similarity of the fasta, therefore of the nucleotide sequences, see Methods; Fig. 1B). Most sequenced genomes resemble the lineage B.20 (see methods). We evaluated whether any of the analyzed employees was part of an epidemiologically linked cluster based on illness onset date, positive test status, and work location. We found a correlation between geographic location and mutation set. All employees in the same clusters also had identical or nearly identical consensus genomes, which reflects the low genetic diversity of SARS-CoV-2 at this stage of the pandemic. It is highly unlikely that there are direct transmission pairs in our dataset, but we cannot conclusively rule out coincident transmission linkage. However, the high similarity between one case belong to the group of Bangladeshi (bang 2B) to the group of Fiumicino, suggests that 2B acted as a bridge between the two clusters. All consensus sequences have been submitted to GISAID and GeneBank.

2.2. Worldwide geographically distribution of double Spike mutation D614G/S939F

To further analyze the features of the identified SARS-CoV-2 double mutation, we investigated more in detail each single variant S939F and D614G. By interrogating 2019nCoV browser we obtained information for both variants, including number of sequences actually deposited, and population frequency. A prediction of the effects that each allele of the variant might have on each transcript was also evidenced (Fig. 2A). In particular, S939F variant, due to nucleotide change C to T in position 24378 of Spike gene, resulted to be about three hundred times less frequent than

Fig. 2. A. S939F and D614G mutations genomic locations and characteristics by 2019nCoV. The evidence level was graded into I-III according to the number of mutations in high-quality sequences and the density distribution of mutations (population frequency of class I is greater than 0.05, which indicates it is more credible; class II variant sites fall in high-density areas; population frequency of class III is less than 0.05, indicating its low reliability). The Variance Time calculates the population frequency of each mutation site over time, evaluates the variance dispersion of the site by calculating the variance of population frequency at each time point. The Variance Area, calculates the population frequency of each mutation site, evaluates the variance dispersion of the site by calculating the variance of population frequency in each region. The Ensembl Variation - Calculated variant consequences is a prediction of the effects that each allele of the variant may have on each transcript. B-C. Time (upper panel) and Area (lower panel) frequencies of S939F (B) and D614G (C) mutations by 2019nCoV are indicated. Isolates number is indicated in blue, variation frequency is indicated in black. (For interpretation of the references to colour in this figure legend, the reader is referred to the web version of this article.)

A



B

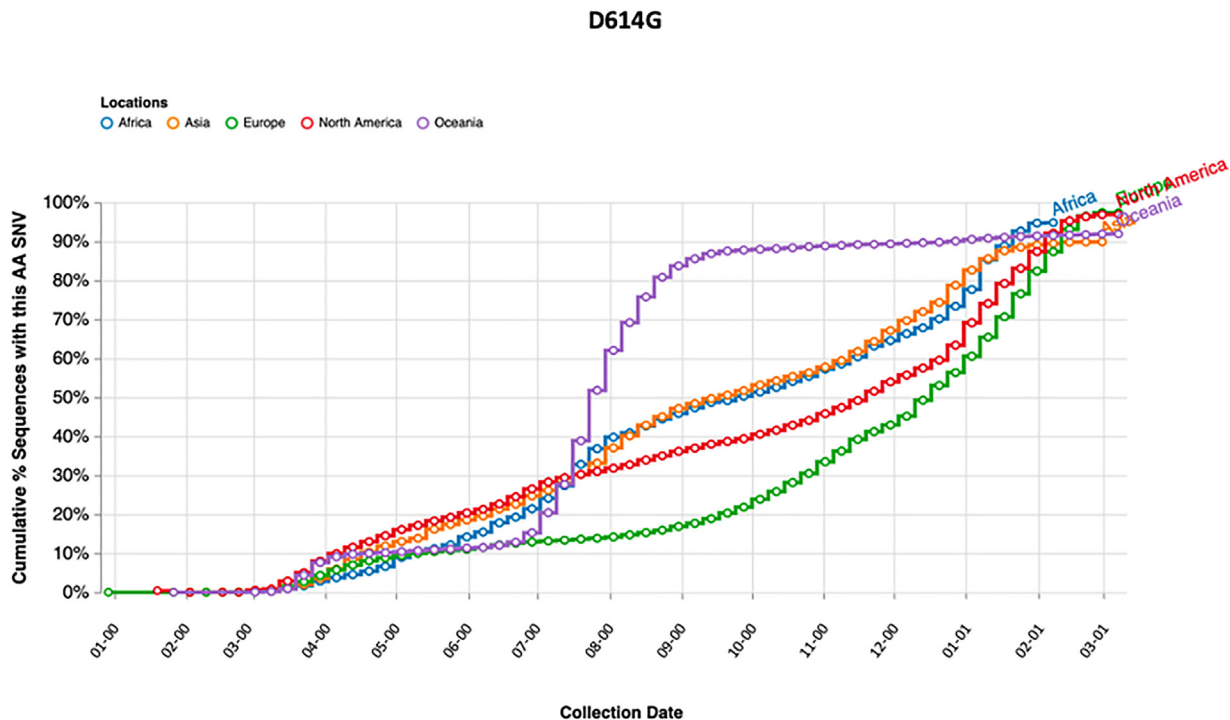
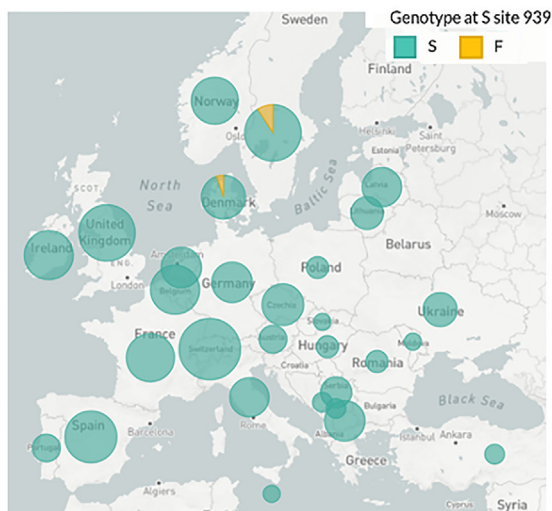


Fig. 3. A-B. S939F (A) and D614G (B) mutations occurrence in the five continents of the world from 1 March 2020 to 31 January 2021 by COVID CG.

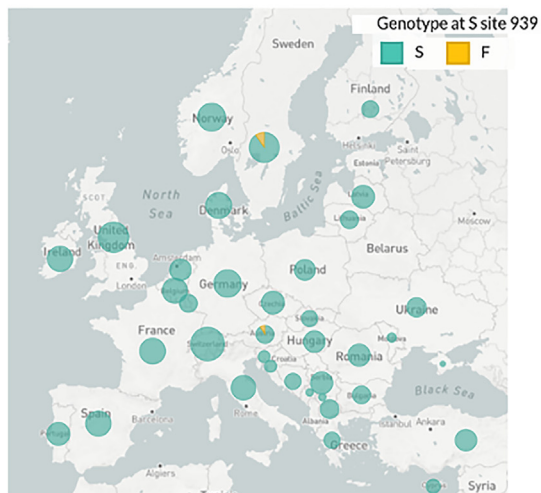
D614G variant, due to nucleotide change A to G in position 23403 (3853 versus 1218522 counts), determining an evidence level of IV for S939F versus I for D614G. Furthermore, we investigated dynamic patterns of SARS-CoV-2 genomic variants S939F and D614G independently, across different sampling locations over

time. As shown in Fig. 2B-C, S939F variant frequency slightly increased over time, reaching 0.0032 at the beginning of June 2021, while D614G variant frequency dramatically increased from 0 at the end of February 2020 to 0.98 at the beginning of June 2021, indicating that this mutated genotype might have higher transmis-

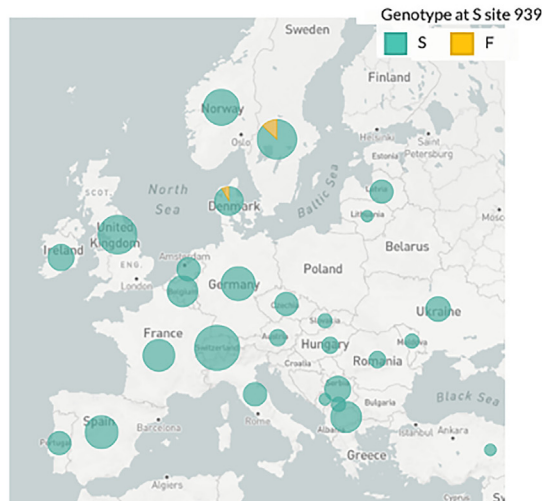
A 1 June – 1 August 2020 (Sweden and Denmark)



B 19 March-13 June 2020 (Sweden and Austria)



16 June- 8 October 2020 (Sweden and Denmark)



C 10 June 2021 (last update)

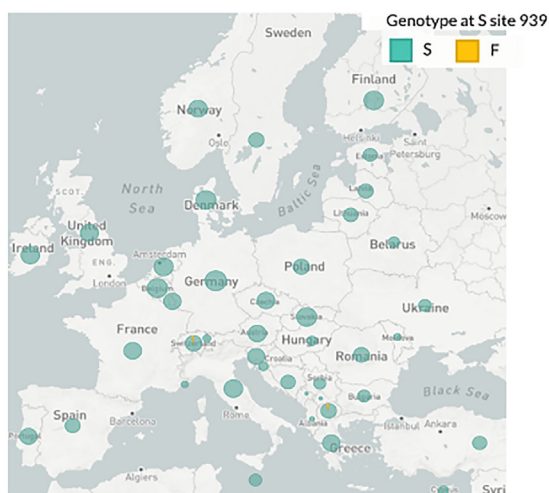


Fig. 4. A-C. S939F mutation distribution (indicated in yellow) in Europe at the indicated time intervals by GSAID. (For interpretation of the references to colour in this figure legend, the reader is referred to the web version of this article.)

sibility. To figure out where S939F and D614G variants were globally located over time, we interrogated COVID-19 CoV Genetics browser. As shown in Fig. 3A–B both variants resulted to be detected in all continents. Indeed, both are still present in Europe (Fig. 3A–B). Subsequently we assessed S939F variant distribution in Europe. Similar to the analysis performed by Korber and collaborators for the global distribution of D614G variant, we interrogated GISAID to assess S939F variant distribution in Europe [8]. We found that S939F variant was detected in Sweden and Denmark when we evidenced S939F-D614G double mutation in our patient samples, (Fig. 4A). Before (from March to June), it was present in Sweden and Austria (Fig. 4B), while to date it has been detected only in Switzerland and North Macedonia (Fig. 4C).

Altogether our findings represent the first evidence of a SARS-CoV-2 variant carrying double Spike D614G/S939F in Italy.

2.3. Unlike D614G, S939F affects T-cell propensity

The Spike D614G/S939F double mutation is poorly studied and consequently its impact on host infection and patient clinical implications are scarcely known. Here we aim to estimate the effects of the D614G/S939F mutations on the immune response. To this end we adapted to the present experimental aim a computational strategy previously introduced to study the SARS-CoV-2 virus and other similar coronaviruses [9,10]. In particular, we considered all the potential epitopes associated with the reference and mutated SARS-CoV-2 spike protein. As reported in La Porta & Zapperi 2020 and La Porta & Zapperi 2021, the first step of the process involved a simulation of proteasome activity and the identification of possible cleavage sites along the protein [9,11,12]. This resulted in a set of 1549 peptides of length 8–11 for the reference spike protein and 1541 total peptides for both mutations in the protein. We then analyzed the peptides searching for likely epitopes using NetTepi which produced a combined score involving binding affinity, peptide stability and T-cell propensity for 13 supported HLA call I [11]. These three measurements all contribute to the potential that a peptide is a T-cell epitope: binding affinity measures the

likelihood that a peptide binds with an HLA, peptide stability measures the ability for the HLA to retain the peptide and T-cell propensity measures whether a peptide is likely to be recognized by a T-cell [11]. The combined score is calculated as a weighted sum of binding affinity, stability and T-cell propensity prediction scores [11]. A high score indicates that the peptide is likely to become a T-cell epitope. From the ranked list of potential epitopes, we selected and counted the highly ranking peptides associated to each HLA allele, as described in the method section. Fig. 5 reports that mutations change the number of potential epitopes for some HLA alleles. In particular, the number of highly ranked peptides is increased by the mutations for HLA-A03:01, HLA-A11:01 and HLA-A26:01, it is decreased for HLA-A02:01, HLA-B39:01 and HLA-B40:01, and it remains unchanged for the other HLA alleles.

The two point mutations D614G and S939F only affected a limited number of peptides, and due to their distance along the sequence no peptide can have more than one mutation. We thus consider the effect of each mutation separately. As shown in Fig. 6A, we can identify a small number of peptides that are either present exclusively in the reference protein (16 for D614G and 20 for S939F) or in the mutated protein (16 for D614G and 12 for S939F) (Table S2). We therefore studied the relevance of these peptides for the immune response. Fig. 6B shows that the T-cell propensity did not change significantly for peptides under the D614G mutation, while the S939F displays a small but significant effect. In particular, the higher T-cell propensity indicates that the mutated spike is more easily recognized by T-cells. In Fig. 6C, we show the combined scores of reference and mutated peptides for the different HLA alleles with some differences observed in an allele dependent manner. In this figure, a decrease in combined score means that the peptide is less likely to be a T-cell epitope.

Notice that the number of alleles available for NetTepi is rather limited. We report in Table S3 the distribution of HLA-A and HLA-B alleles found in a Bangladeshi population extracted from the allele-frequencies.net website. We can see that NetTepi HLA-A alleles represent 62% of the population and HLA-B only 50%. To obtain a larger coverage of the alleles present in the population we

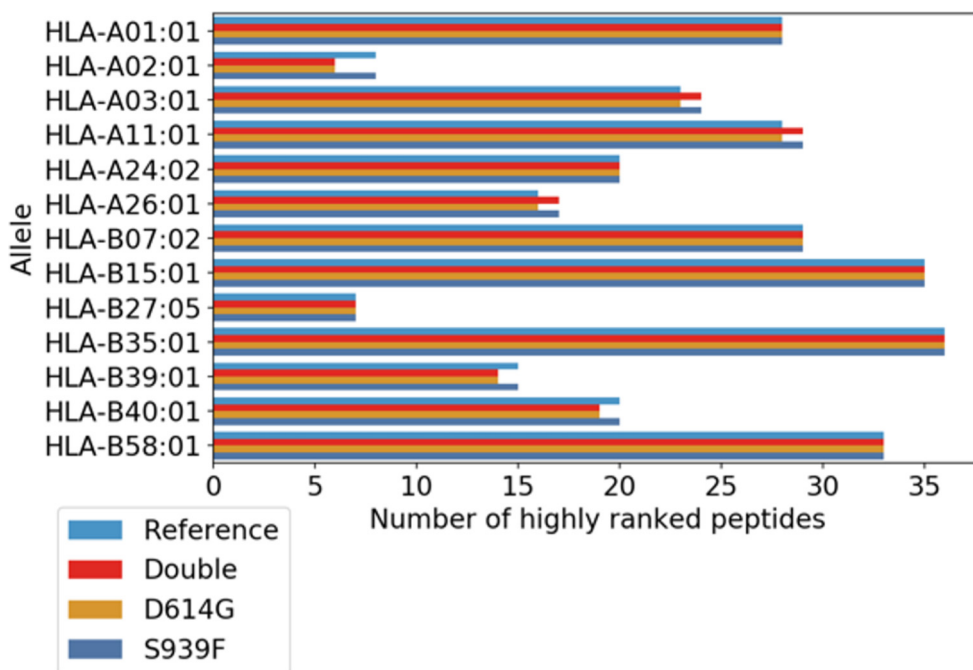


Fig. 5. Mutations affect the number of likely T-cell epitopes in a HLA-dependent manner. The figure shows the number of highly ranked peptides from the reference and the mutated (D614G and S939F) SARS-CoV-2 spike protein for a set of HLA alleles, estimated with NetTepi as discussed in the Methods section. For some HLA alleles, the number of highly ranked peptides, the potential T-cell epitopes, differs for the reference and the mutated virus.

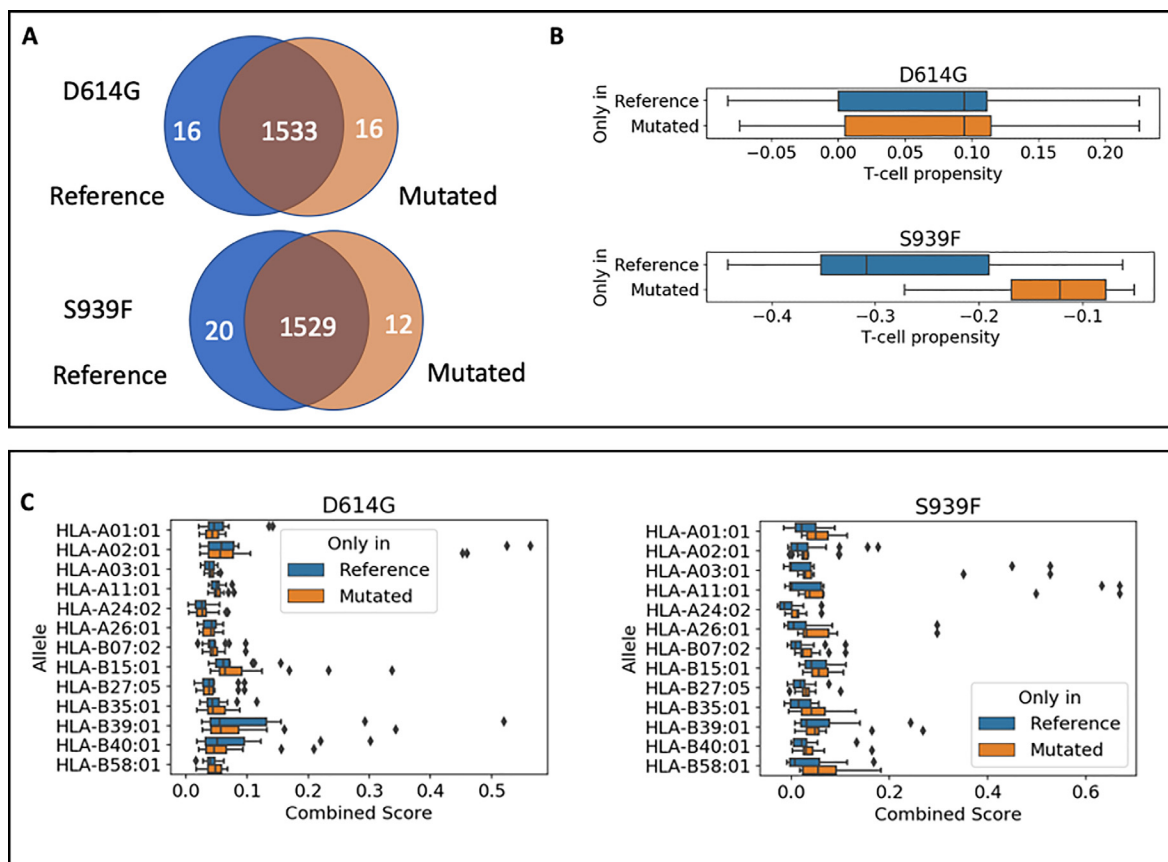


Fig. 6. Difference in T-cell propensity and T-cell epitope combined score between reference and mutated peptides. A. After proteasome cleavage simulation, we obtain 1513 peptides that are common between the reference and the mutated virus. A small number of peptides are only present either in the reference virus or in the mutated virus. B. The distribution of T-cell propensities estimated by NetTepi is not affected by the D614G mutation ($p = 0.99$ according to the Kolmogorov-Smirnov test) while a significant change is observed for the S939F mutation ($p = 0.01$ according to the Kolmogorov-Smirnov test). The boxplot reports median and quartiles of the data. C. The mutations affect the T-cell epitope combined score of the peptides estimated by NetTepi in a HLA-dependent manner.

expanded the analysis by considering MHCflurry 2.0 that is able to predict the binding affinity of arbitrary peptides to any HLA molecule using an artificial neural network [13]. We used this tool to compare the binding affinity of the small group of reference and mutated peptides discussed above for 26 HLA class I alleles providing a broad coverage of the human population (see Fig. S1 for a Venn diagram reporting the alleles considered and for a comparison between the predictions of NetTepi and MHCflurry). In particular, these 26 alleles represent 93% of the Bangladeshi population for HLA-A alleles and 72% for HLA-B alleles. The results reported in Fig. 7A-B show that mutations change the binding landscape only in some cases. For example in the case of the S939F, we could identify some alleles where some new strongly binding peptides emerged in the mutated protein (e.g. HLA-A26:01 or HLA-A32:01), while for the D614G mutation the presence of isolated strongly binding peptides was not affected by the presence of isolated strongly binding peptides (see HLA-A02:01, HLA-A02:03 and HLA-A02:06).

In aggregate, our findings indicate that Spike mutations may potentially alter CD8 T cell immune response to SARS-CoV-2 thereby affecting the rate of infection and clinical impact.

3. Discussion

The widespread diffusion of SARS-CoV-2 depends, at least in part, from its high rate of genome mutation that leads to the appearance of viral variants with different rate of infection and severity of the Covid 19 disease. As for cancer, whose deep deci-

phering of DNA mutational landscape has been pivotal for the identification of specific driver mutations and for the design of precision medicine therapeutic approaches, the sequencing of the viral genome by using NGS technologies is of pivotal importance.

In the present manuscript, retrospective NGS of SARS-CoV-2 viral genomes revealed a double Spike mutation D614G/S939F in the members of Bangladeshi community located in Ostia as occasional employees. This is the first evidence of the presence of this SARS-CoV-2 double Spike mutation in Italy. Its presence in Europe was previously found in Denmark, Sweden and Croatia. These findings further emphasize the critical need, which is still unmet, to perform massive next generation sequencing of SARS-CoV-2 viral genome to monitor the appearance of novel viral variants and to predict their rate of infection and severity of the related illness in the infected people.

Pre-clinical evidence showed that D614G/S939F double Spike mutation was among those mutations that exhibited higher rate of infection [14]. Multiple studies suggest that T cells are important in the immune response against SARS-CoV-2, and may mediate long-term protection against the virus [15–19]. Interestingly, we provide novel evidence that the described double Spike mutation affects immune response. To this end, we use computational methods based on artificial neural networks such as NetTepi [11] and MHCflurry [13]. Indeed, a combined score involving binding affinity, peptide stability and T-cell propensity for 13 supported HLA class I alleles was generated (11). This led to the evaluation of T cell propensity that resulted slight but significantly modulated upon

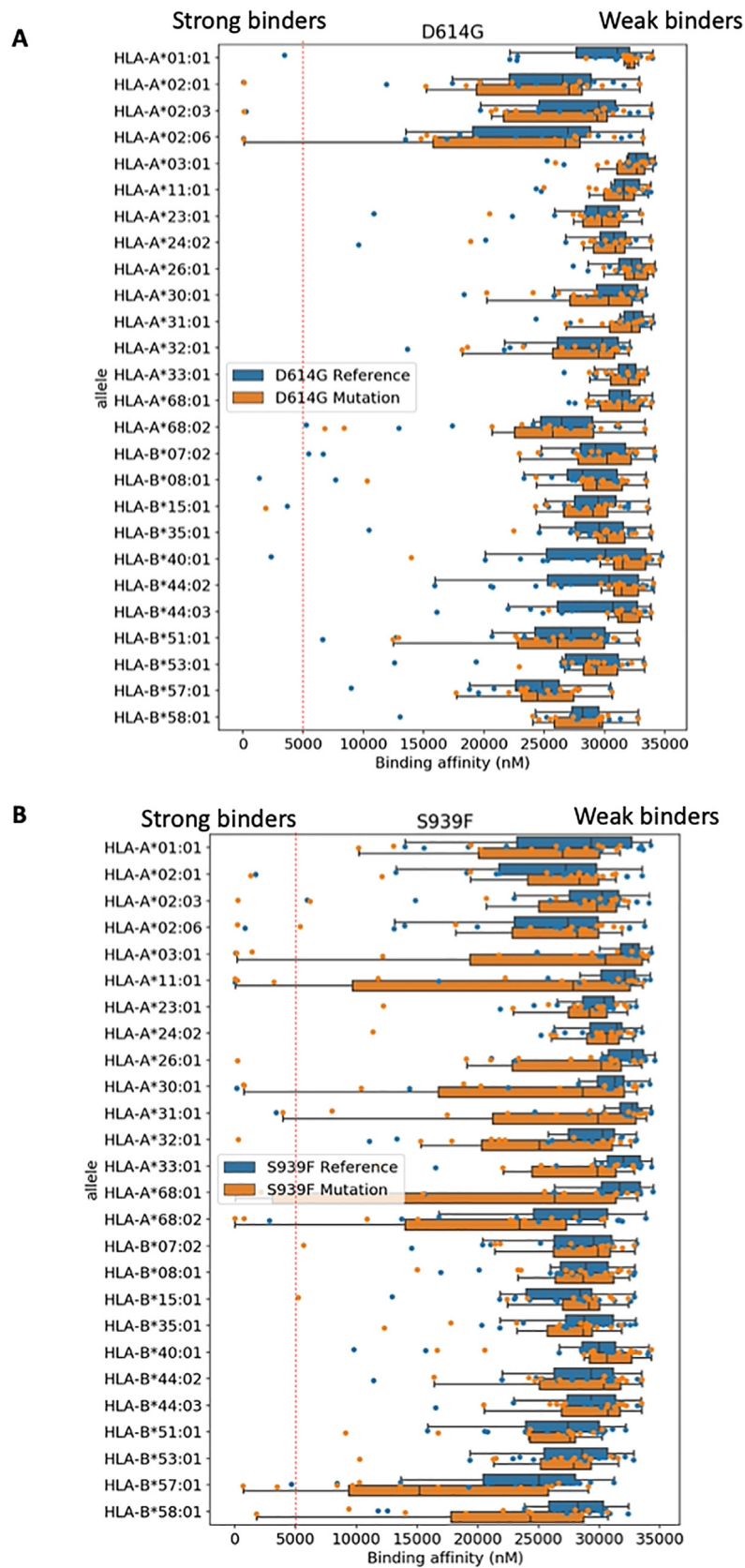


Fig. 7. Effect of mutations on binding affinities for a broad range of HLA alleles. We report the binding affinities for the peptides only present in the reference and in the mutated spike protein obtained using MHCflurry 2.0. Individual peptides binding affinities are reported as dots. The boxplot reports median and quartiles of the same data. A. D614G mutation. B. S939F mutation.

S939F mutation compared to D614G. Furthermore, the binding landscape affinity of predicted

peptides to any HLA molecules was affected by S939F mutation when compared to D614G mutation, that, on the contrary, had no impact on the affinity of strongly binding peptides. One of the most debated issues within the SARS-CoV-2 community is the efficacy of the currently used vaccines against specific viral variants. The generation of tools, as those applied for the identification of a combined score have potential utility as they might also predict viral immune escape of specific SARS-CoV-2 variants. We should also notice that HLA-binding algorithms are widely used in the literature but the results provide only a first indication that particularly in the case of SARS-CoV-2 should eventually be validated experimentally [20]. To date a major question in the SARS-CoV-2 arena relies on the efficacy of the existing vaccines to neutralize emerging viral variants. This emphasizes the need of generating flexible and rapid tools of prediction of immune response upon SARS-CoV-2 infection to instruct not only vaccines but also other antiviral therapeutic approaches.

Collectively, the massive NGS sequencing of viral genomes which leads to the identification of emerging viral variants and the combined evaluation of their impact on the immune response of the infected subject will have a paramount role in fighting both SARS-CoV-2 diffusion and vaccine efficacy.

4. Methods

4.1. Viral RNA extraction by San Gallicano Institute

RNAs extraction from nasopharyngeal and oropharyngeal swab was performed in two ways. First (to perform routinely Real-Time PCR) by using Bosphore EX-Tract Dry Swab RNA Solution (AnatoliaGeneWork) according to manufacturer's instructions. Briefly, a dry throat swab from the patient was added to the EX-Tract RNA Solution and vortexed for 60 s. A proportion of this solution was then heated at 95 °C for 8 min. Once cooled this was added directly to the PCR mastermix. Second (to perform NGS), by using the QIASymphony Virus/Pathogen Kit (QIAGEN), with a final elution of 60ul.

4.2. SARS-CoV-2 detection by San Gallicano Institute

For the detection of SARS-CoV-2 in RNAs extracted from nasopharyngeal and oropharyngeal swab we used Bosphore Novel Coronavirus (2019-nCoV) Detection Kit v2 (AnatoliaGeneWork). This kit is a Real-Time PCR-based in vitro diagnostic medical device that allows to detect two regions of the virus in two separate reactions: E gene is used for screening purpose, where 2019-nCoV and also the closely related coronaviruses are detected, and the orf1ab target region is used to discriminate 2019-nCoV specifically. This kit includes also an internal control in order to check RNA extraction, PCR inhibition and application errors.

4.3. SARS-CoV-2 detection by genoma laboratory (qualitative analysis)

For the detection of presence/absence of COVID-19, 10 ul of RNA was tested using Allplex™ 2019-nCoV Assay (Seegene) according to manufacturer's instructions.

The real-time RT-PCR was performed on the CFX96™ (BioRad, California, USA) platform, and subsequently interpreted by Seegene's Viewer software.

4.4. SARS CoV-2 NGS sequencing

Around 5–10 ng of each viral RNA sample was reverse transcribed using SuperScript™ VILO™ cDNA Synthesis Kit (Thermo

Fisher Scientific) following the instructions of the Ion Torrent™ Ion AmpliSeq™ Library Kit Plus protocol (Thermo Fisher Scientific). cDNAs have been used for the virus amplification throughout the “Ion AmpliSeq SARS-CoV-2 Research Panel” by AmpliSeq™ Technology (Thermo Fisher Scientific). Depending on the number of copies of virus in the extracted samples from 20 to 27 PCR cycles have been performed to get amplicons spanning the virus genome. After the first step of PCR amplification library preparation has been conducted following the Ion Torrent™ Ion AmpliSeq™ Library Kit Plus protocol (Thermo Fisher Scientific). SARS-CoV-2 AmpliSeq libraries have been sequenced by using the Ion Chef™ and the Ion Genestudio™ S5 Plus Systems (Thermo Fisher Scientific). Several Ion-supported plug-ins installed in Torrent Suite Software (Thermo Fisher Scientific) have been used for bioinformatic analysis to provide data on coverage sequencing (Table S1), variant calling and annotation, and genome assembly: CoverageAnalysis; VariantCaller, Covid19AnnotateSNPEff, IRMA and AssemblerTrinity [21–24].

We calculated the mean depth of coverage from the 13 BAM files, at single nucleotide resolution using bed tools. Mapped Reads: number of reads mapped to viral genome; Filtered Reads: percentage of reads failing mapping step; Target Reads: percentage of reads mapped to viral genome; Mean Depth: mean number of time a region has been sequenced; Uniformity: percentage of reads with at least 0.2x of average coverage.

All consensus sequences have been submitted to GISAID with the following accession IDs: EPI_ISL_1181628, EPI_ISL_1257897, EPI_ISL_1224910, EPI_ISL_1257867, EPI_ISL_1257868, EPI_ISL_1257869, EPI_ISL_1257870, EPI_ISL_1257871, EPI_ISL_1257872, EPI_ISL_1257873, EPI_ISL_1257894, EPI_ISL_1257895, EPI_ISL_1257896.

4.5. Bioinformatic characterization of S939F and D614G variants

Information about S939F and D614G variants counts and frequency were obtained by 2019nCoV browser (<https://bigd.big.ac.cn/ncov>) [25–27].

Distribution of S939F and D614G variants in the world over time was provided by COVID-19 CoV Genetics browser (<https://covidcg.org>) [28].

Distribution of S939F variant in Europe at the indicated time points was verified by interrogating GISAID database (<https://www.gisaid.org>) [29].

4.6. Peptide selection by proteasome cleavage.

In the following analysis, we only consider peptides that are likely to be produced by proteasome degradation using NetChop 3.1 [12] a neural network based algorithm that scans proteins for probable cleavage sites of the human proteasome. We perform the scan for the spike protein of the reference virus SARS-CoV-2 and of the mutated virus which includes the two mutations D614G and S939F.

4.7. Identification of T cell epitopes

Potential T cell epitopes are identified using NetTepi 1.0 through the server (<https://services.healthtech.dtu.dk/service.php?NetTepi-1.0>). The method combines estimates for peptide-HLA binding affinity, peptide-HLA stability and T cell propensity [11]. Peptides are then ranked against a set of 200,000 natural peptides to obtain a global rank score. Here we scan all the peptides selected by proteasome simulation with lengths 8–11 from the spike protein of the reference virus SARS-CoV-2 and of the mutated virus, including the two mutations D614G and S939F.

We select highly ranked peptides as those with rank score lower than 2% which are considered “strong binders” (<0.5%) and “weak binders” (<2%). We perform the calculations for all the class I MHC alleles supported by NetTepi, using the default values for the relative weight on stability prediction and the relative weight on T cell propensity prediction.

4.8. Prevalence of HLA alleles

The prevalence of HLA alleles in the Bangladeshi population has been identified using Allele frequency net database (AFND) [30].

4.9. Estimate of binding affinities

Binding affinities are estimated using MHC flurry 2.0 [13]. We only estimate the binding affinities for peptides selected by proteasome using NetChop 3.1 and that differ between the reference and the mutated (D614G and S939F) SARS-CoV-2 virus.

CRedit authorship contribution statement

Sara Donzelli: Investigation, Writing – review & editing. **Francesca Spinella:** Investigation. **Enea Gino di Domenico:** Investigation. **Martina Pontone:** Investigation. **Iliaria Cavallo:** Investigation. **Giulia Orlandi:** Investigation. **Stefania Iannazzo:** Investigation. **Giulio Maria Ricciuto:** Investigation. **ISG Virology Covid Team:** Investigation. **Raul Pellini:** Investigation. **Paola Muti:** Writing – review & editing. **Sabrina Strano:** Writing – review & editing. **Gennaro Ciliberto:** Supervision. **Fabrizio Ensoli:** Writing – review & editing. **Stefano Zapperi:** Investigation, Writing – review & editing. **Caterina A.M. La Porta:** Investigation, Writing – review & editing. **Giovanni Blandino:** Conceptualization, Writing – review & editing, Supervision, Project administration. **Aldo Morrone:** Supervision. **Fulvia Pimpinelli:** Conceptualization, Writing – review & editing, Supervision, Project administration.

Declaration of Competing Interest

The authors declare that they have no known competing financial interests or personal relationships that could have appeared to influence the work reported in this paper.

Acknowledgments

We gratefully acknowledge all the Authors from the Originating laboratories responsible for obtaining the specimens and the Submitting laboratories where genetic sequence data were generated and shared via the GISAID Initiative, on which this research is based.

Appendix A. Supplementary data

Supplementary data to this article can be found online at <https://doi.org/10.1016/j.csbj.2022.01.021>.

References

- Ye Z-W, Yuan S, Yuen K-S, Fung S-Y, Chan C-P, Jin D-Y. Zoonotic origins of human coronaviruses. *Int J Biol Sci* 2020;16(10):1686–97.
- Peiris JSM, Guan Y, Yuen KY. Severe acute respiratory syndrome. *Nat Med* 2004;10(S12):S88–97.
- Alsolamy S, Arabi YM. Infection with Middle East respiratory syndrome coronavirus. *Can J Respir Ther*. 2015;51(4):102.
- Hoffmann M, Kleine-Weber H, Schroeder S, Krüger N, Herrler T, Erichsen S, et al. SARS-CoV-2 cell entry depends on ACE2 and TMPRSS2 and is blocked by a clinically proven protease inhibitor. *Cell* 2020;181(2):271–280.e8.
- Ou X, Liu Y, Lei X, Li P, Mi D, Ren L, et al. Characterization of spike glycoprotein of SARS-CoV-2 on virus entry and its immune cross-reactivity with SARS-CoV. *Nat Commun* 2020;11(1). <https://doi.org/10.1038/s41467-020-15562-9>.
- Sakkiah S, Guo W, Pan B, Ji Z, Yavas G, Azevedo M, et al. Elucidating interactions between SARS-CoV-2 trimeric spike protein and ACE2 using homology modeling and molecular dynamics simulations. *Front Chem* 2020;8. <https://doi.org/10.3389/fchem.2020.622632>.
- Chan YA, Zhan SH. The emergence of the spike furin cleavage site in SARS-CoV-2. *Mol Biol Evol* 2021;msab327.
- Korber B, Fischer WM, Gnanakaran S, Yoon H, Theiler J, Abfalterer W, et al. Tracking changes in SARS-CoV-2 spike: evidence that D614G increases infectivity of the COVID-19 virus. *Cell* 2020;182(4):812–827.e19.
- La Porta CAM, Zapperi S. Estimating the binding of Sars-CoV-2 peptides to HLA Class I in human subpopulations using artificial neural networks. *Cell Syst*. 2020;11(4):412–417.e2.
- La Porta CAM, Zapperi S. SARS-CoV-2 variants-Immune profile of SARS-CoV-2 variants of concern *Frontiers in Digital Health*. 2021;in press.
- Trolle T, Nielsen M. NetTepi: an integrated method for the prediction of T cell epitopes. *Immunogenetics*. 2014;66(7-8):449–56.
- Nielsen M, Lundegaard C, Lund O, Kesmir C. The role of the proteasome in generating cytotoxic T-cell epitopes: insights obtained from improved predictions of proteasomal cleavage. *Immunogenetics* 2005;57(1-2):33–41.
- O'Donnell TJ, Rubinsteyn A, Laserson U. MHCflurry 2.0: improved Pan-allele prediction of MHC Class I-presented peptides by incorporating antigen processing. *Cell Syst*. 2020;11(1):42–48.e7.
- Li Q, Wu J, Nie J, Zhang Li, Hao H, Liu S, et al. The impact of mutations in SARS-CoV-2 Spike on viral infectivity and antigenicity. *Cell* 2020;182(5):1284–1294.e9.
- Braun J, Loyal L, Frensch M, Wendisch D, Georg P, Kurth F, et al. SARS-CoV-2-reactive T cells in healthy donors and patients with COVID-19. *Nature* 2020;587(7833):270–4. <https://doi.org/10.1038/s41586-020-2598-9>.
- Grifoni A, Weiskopf D, Ramirez SI, Mateus J, Dan JM, Moderbacher CR, et al. Targets of T cell responses to SARS-CoV-2 coronavirus in humans with COVID-19 disease and unexposed individuals. *Cell* 2020;181(7):1489–1501.e15. <https://doi.org/10.1016/j.cell.2020.05.015>.
- Le Bert N, Tan AT, Kunasegaran K, Tham CYL, Hafezi M, Chia A, et al. SARS-CoV-2-specific T cell immunity in cases of COVID-19 and SARS, and uninfected controls. *Nature* 2020;584(7821):457–62. <https://doi.org/10.1038/s41586-020-2550-z>.
- Peng Y, Mentzer AJ, Liu G, Yao X, Yin Z, Dong D, et al. Broad and strong memory CD4+ and CD8+ T cells induced by SARS-CoV-2 in UK convalescent individuals following COVID-19. *Nat Immunol* 2020;21(11):1336–45. <https://doi.org/10.1038/s41590-020-0782-6>.
- Sekine T, Perez-Potti A, Rivera-Ballesteros O, Strålin K, Gorin J-B, Olsson A, et al. Robust T cell immunity in convalescent individuals with asymptomatic or mild COVID-19. *Cell* 2020;183(1):158–168.e14. <https://doi.org/10.1016/j.cell.2020.08.017>.
- Sohail MS, Ahmed SF, Quadeer AA, McKay MR. In silico T cell epitope identification for SARS-CoV-2: Progress and perspectives. *Adv Drug Deliv Rev* 2021.
- Shepard SS, Meno S, Bahl J, Wilson MM, Barnes J, Neuhaus E. Viral deep sequencing needs an adaptive approach: IRMA, the iterative refinement meta-assembler. *BMC Genomics* 2016;17:708. <https://doi.org/10.1186/s12864-016-3030-6>.
- Haas BJ, Papanicolaou A, Yassour M, Grabherr M, Blood PD, Bowden J, et al. De novo transcript sequence reconstruction from RNA-seq using the Trinity platform for reference generation and analysis. *Nat Protoc* 2013;8(8):1494–512.
- Grabherr MG, Haas BJ, Yassour M, Levin JZ, Thompson DA, Amit I, et al. Full-length transcriptome assembly from RNA-Seq data without a reference genome. *Nat Biotechnol* 2011;29(7):644–52.
- Cingolani P, Platts A, Wang LL, Coon M, Nguyen T, Wang L, et al. A program for annotating and predicting the effects of single nucleotide polymorphisms, SnpEff: SNPs in the genome of *Drosophila melanogaster* strain w1118; iso-2; iso-3. *Fly* 2012;6(2):80–92.
- Song S, Ma L, Zou D, Tian D, Li C, Zhu J, et al. The Global Landscape of SARS-CoV-2 genomes, variants, and haplotypes in 2019nCoV. *Genomics Proteomics Bioinformatics* 2020.
- Ray Stricklin W, Mench JA. Social organization. *Vet Clin North Am Food Anim Pract* 1987;3(2):307–22.
- Zhao WM, Song SH, Chen ML, Zou D, Ma LN, Ma YK, et al. The 2019 novel coronavirus resource. *Yi Chuan* 2020;42(2):212–21.
- Shu Y, McCauley J. GISAID: Global initiative on sharing all influenza data - from vision to reality. *Euro Surveill* 2017;22(13).
- Elbe S, Buckland-Merrett G. Data, disease and diplomacy: GISAID's innovative contribution to global health. *Glob Chall* 2017;1(1):33–46.
- Gonzalez-Galarza F, McCabe A, Santos ED, Jones J, Takeshita L, Ortega-Rivera N, et al. Allele frequency net database (AFND) 2020 update: gold-standard data classification, open access genotype data and new query tools. *Nucl Acids Res* 2020. <https://doi.org/10.1093/nar/gkz1029>.
- Sievers F, Higgins DG. Clustal Omega for making accurate alignments of many protein sequences. *Protein Sci* 2018;27(1):135–45.
- Sievers F, Wilm A, Dineen D, Gibson TJ, Karplus K, Li W, et al. Fast, scalable generation of high-quality protein multiple sequence alignments using Clustal Omega. *Mol Syst Biol* 2011;7(1):539. <https://doi.org/10.1038/msb.2011.75>.

- [33] Kumar S, Stecher G, Li M, Knyaz C, Tamura K. MEGA X: Molecular Evolutionary Genetics Analysis across Computing Platforms. *Mol Biol Evol.* 2018;35(6):1547–9.
- [34] Chernomor O, von Haeseler A, Minh BQ. Terrace Aware Data Structure for Phylogenomic Inference from Supermatrices. *Syst Biol* 2016;65(6):997–1008.
- [35] Nguyen LT, Schmidt HA, von Haeseler A, Minh BQ. IQ-TREE: a fast and effective stochastic algorithm for estimating maximum-likelihood phylogenies. *Mol Biol Evol* 2015;32(1):268–74.